



HAL
open science

Design study of the coupling of an air gap membrane distillation unit to an air conditioner

Ahmadou Tidiane Diaby, Paul Byrne, Patrick Loulergue, Béatrice Balannec,
Anthony Szymczyk, Thierry Maré, Ousmane Sow

► **To cite this version:**

Ahmadou Tidiane Diaby, Paul Byrne, Patrick Loulergue, Béatrice Balannec, Anthony Szymczyk, et al.. Design study of the coupling of an air gap membrane distillation unit to an air conditioner. Desalination, 2017, 420, pp.308 - 317. 10.1016/j.desal.2017.08.001 . hal-01579519

HAL Id: hal-01579519

<https://hal.science/hal-01579519>

Submitted on 31 Aug 2017

HAL is a multi-disciplinary open access archive for the deposit and dissemination of scientific research documents, whether they are published or not. The documents may come from teaching and research institutions in France or abroad, or from public or private research centers.

L'archive ouverte pluridisciplinaire **HAL**, est destinée au dépôt et à la diffusion de documents scientifiques de niveau recherche, publiés ou non, émanant des établissements d'enseignement et de recherche français ou étrangers, des laboratoires publics ou privés.

Manuscript Details

Manuscript number	DES_2017_1223
Title	Design study of the coupling of an air gap membrane distillation unit to an air conditioner
Article type	Full Length Article

Abstract

This work presents the design of a membrane distillation (MD) unit coupled to a refrigeration device. The operation of an MD pilot plant is first tested then modelled using EES software. The range of hot water feed temperature provided by the condenser of the refrigeration device may vary from 25 to 65 °C as needed by the MD unit. The results of the experimental study enable to validate a 1D theoretical model with a maximum deviation of $\pm 6\%$. This model is coupled to a heat pump model to simulate the operation of a coupled machine. The system performance is studied following two scenarios. In Scenario 1 (continuous mode), the system is connected to a seawater network. In Scenario 2 (batch mode), the seawater reservoir is filled up manually every day. The simulation study shows that the increase of the feed water temperature enhances significantly the produced permeate flux but decreases the performance of the heat pump. This system exhibits high exergy efficiency and GOR for a high feed water temperature. Exergy efficiency and gained output ratio (GOR) decrease as the water flow increases and the hot water temperature decreases. Conversely, the coefficient of performance (COP) of the refrigerator increases.

Keywords	air conditioner; coupling; air gap membrane distillation
Corresponding Author	Paul Byrne
Order of Authors	Ahmadou Diaby, Paul Byrne, Patrick LOULERGUE, Beatrice Balannec, Anthony SZYMCZYK, Thierry Maré, Ousmane Sow
Suggested reviewers	A.G Fane, Wojciech Kujawski, NALAN KABAY

Submission Files Included in this PDF

File Name [File Type]

Cover Letter.doc [Cover Letter]

Diaby Desalination.docx [Manuscript File]

To view all the submission files, including those not included in the PDF, click on the manuscript title on your EVISE Homepage, then click 'Download zip file'.

Paul Byrne
IUT Génie Civil
Civil & Mechanical Engineering Laboratory
3 Rue du Clos Courtel
BP 90422
35704 Rennes Cedex 7
France
paul.byrne@univ-rennes1.fr
Tel : +33 2 23 23 42 97
Fax : +33 2 23 23 40 51

Rennes, 09/06/17

To editor and reviewers of Desalination

Subject: Cover letter

Dear Editor, dear reviewers,

Please find in this submission a full-length article on the design study of the coupling of a cooling device with an air gap membrane distillation unit. This work was presented at the MEMDES 2017 conference in Las Palmas de Gran Canaria. The first author is Ahmadou Diaby, a PhD student under the co-supervision of researchers from LGCGM and ISCR laboratories from Rennes France and the LEA of Dakar Senegal.

Best regards,

Paul Byrne

Design study of the coupling of an air gap membrane distillation unit to an air conditioner

Ahmadou Tidiane Diaby^{1,2}, Paul Byrne^{1*}, Patrick Loulergue³, Béatrice Balanec³, Anthony Szymczyk³,
Thierry Maré¹, Ousmane Sow²

¹Laboratoire Génie Civil Génie Mécanique, INSA de Rennes et Université de Rennes 1, France

²Laboratoire d'Energétique Appliquée, Ecole Supérieure Polytechnique, Université Cheikh Anta Diop de
Dakar, Sénégal

³Institut des Sciences Chimiques de Rennes (UMR CNRS 6226), Université de Rennes 1, ENSCR, France
*paul.byrne@univ-rennes1.fr

Abstract

This work presents the design of a membrane distillation (MD) unit coupled to a refrigeration device. The operation of an MD pilot plant is first tested then modelled using EES software. The range of hot water feed temperature provided by the condenser of the refrigeration device may vary from 25 to 65 °C as needed by the MD unit. The results of the experimental study enable to validate a 1D theoretical model with a maximum deviation of $\pm 6\%$. This model is coupled to a heat pump model to simulate the operation of a coupled machine.

The system performance is studied following two scenarios. In Scenario 1 (continuous mode), the system is connected to a seawater network. In Scenario 2 (batch mode), the seawater reservoir is filled up manually every day. The simulation study shows that the increase of the feed water temperature enhances significantly the produced permeate flux but decreases the performance of the heat pump. This system exhibits high exergy efficiency and GOR for a high feed water temperature. Exergy efficiency and gained output ratio (GOR) decrease as the water flow increases and the hot water temperature decreases. Conversely, the coefficient of performance (COP) of the refrigerator increases.

Keywords: air conditioner, coupling, air gap membrane distillation

1. Introduction

The building sector accounts for 40% of the world's energy consumption. The number of air conditioning and refrigeration devices is estimated at 4 billion units consuming 17 % of global electric energy [1]. When installed in high buildings, air conditioners heat air flowing through the outdoor condensers. The air density increases and the air tends to flow up near another condenser to be heated again. This phenomenon is partly responsible for the urban heat island effect. The proximity of buildings and their cooling equipment creates hot outdoor environment provoking higher cooling demands and lower performance of air conditioners. In addition, the world population is growing, which leads to an increase of the needs of commercial and domestic refrigeration and air conditioning as well as in drinking water. Human activities lead to the decrease of available water resources because of pollutions or their use for farming and industrial activities. Over 40% of the world's population living in watersheds by serious water shortages, the demand in terms of water resource levy should increase by around 55% by 2050 [2]. The desalination of seawater or brackish water is often a solution to the lack of fresh water.

Numerous studies deal with cold production for air conditioning or refrigeration firstly and secondly the desalination of seawater. However, there are very few papers in the literature studying the coupling of cooling systems and desalination in order to produce simultaneously a cooling capacity and fresh water (see [3] for a recent review). In addition, the simulation study of a membrane distillation system for seawater desalination coupled to a heat pump was already conducted but needs to be improved in terms of system sizing and operating conditions [4]. An optimization study for the design of thermal distillation systems thermally coupled to treatment facilities was carried out by Gonzalez-Bravo et al. [5] to obtain simultaneously the optimization on a minimum cost criterion of the thermal distillation unit and the heat exchange network that integrates heating and cooling in the process facility.

Figure 1 classifies the main desalination techniques are into two categories: membrane processes and thermal processes. Figure 1 also recalls the percentage of total volume of desalinated water production for the three main systems, which are reverse osmosis (RO), multi-stage flash distillation (MSF) and multiple-effect distillation (MED). The other systems account for the remaining 6 %. The degree of compatibility of desalination techniques with heat pumps is evaluated in Table 1. It appears clearly that the operation of electrodialysis (ED) is not related to heat. The temperature has very low influence on the operation of RO. These two methods of membrane desalination technology are not suited to the coupling with heat pumps. MED and MD appear to be systems

compatible with classic heat pumps. The operating temperature range of MSF is high in comparison to that produced by the heat pump that can range from 25 °C to 65 °C. For thermal vapour compression (TVC), the temperature range corresponds to that of a heat pump, but this process does not have a refrigerating effect.

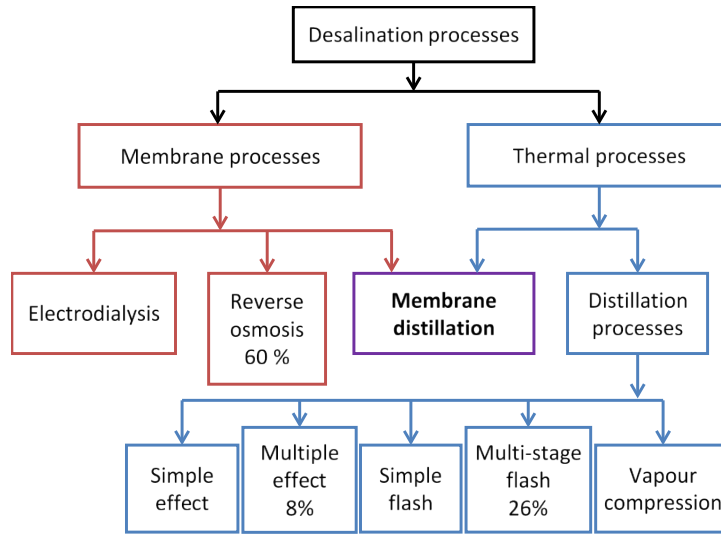


Figure 1: Classification of commonly used desalination technologies

Table 1: Compatibility assessment of desalination systems with refrigerating devices

Systems	Process	Operating temperature	Compatibility with a refrigerating device
ED	Mechanical / Membrane	Not appropriate	No
RO	Mechanical / Membrane	Low influence	No
MED	Thermal	70 °C – 80 °C	Yes, with a high temperature HP
MSF	Thermal	80 °C – 120 °C	No
MD	Thermal / Membrane	40 °C – 80 °C	Yes, with a classic HP
TVC	Mechanical / Thermal	60 °C – 70 °C	No refrigerating effect

Membrane distillation is both a thermal and a membrane process. MD can produce high-quality pure water by utilizing a porous hydrophobic membrane to separate a feed compartment and a permeate compartment. The MD process is most suitable due to the low operating temperatures, compatible with conventional air conditioning units. Low-grade waste heat or renewable energy might be favourably used for seawater desalination using membrane distillation [6]. MD is a thermal membrane process using the vapour pressure gradient created between a hot stream and a cold stream as the driving force. Four classic configurations of MD are usually encountered in the literature, which differ by the nature of the permeate management [7-8]: direct contact membrane distillation (DCMD), air gap membrane distillation (AGMD), vacuum membrane distillation (VMD) and sweeping-gas membrane distillation (SGMD). In all MD configurations, one side of the hydrophobic membrane is in contact with the hot feed solution. The other side is in contact with cold permeate for DCMD, air gap for AGMD, vacuum for VMD and gas for SGMD. DCMD is the easiest and simplest configuration [7]. In this process, the heat loss by conduction is high and it presents a high risk of wetting of the membrane. AGMD is the most versatile of all configurations because of its air gap [9]. It is characterized by the lowest thermal losses and by a lower risk of wetting and fouling of the membrane. The recovery of the heat to preheat the feed solution is easy with DCMD and AGMD. SGMD is known for its low temperature polarization and relatively low permeate flux [7]. VMD has a low loss of thermal conductivity and resistance to mass transfer in the boundary layer with a high permeate flux [10], it has a very high risk of wetting the membrane [11]. Additional energy is consumed for the vacuum pump in VMD and for ventilation in SGMD. The heat recovery is very difficult with these two configurations and the set-up is more complex due to the need of an external condenser. Following this screening of desalination systems, AGMD was chosen for the coupled system due to its simplicity.

Therefore, the objective of this study is to couple a cooling device with an AGMD unit for the simultaneous production of cold air and fresh water by desalination. The thermodynamic cycle of the cooling device and the

AGMD unit were modelled using EES software [12]. Each component of the refrigeration circuit (compressor, condenser, expansion valve and evaporator) is modelled. Based on the experimental results obtained with an AGMD pilot plant (different machine from the coupled system), the model is first validated. It is subsequently used to predict the performance, in terms of permeate flux, energy and exergy efficiency, of the coupled system that produces cooling energy and distilled water.

2. Description of the coupled system

The idea is to recover the heat lost towards the environment by a refrigeration equipment or an air conditioning equipment to produce fresh water (Figure 2). The coupled system is sized using a small air conditioner with a cooling capacity of 2.5 kW. The evaporator supplies cooling energy. This heat exchanger is here a roll-bond in which the refrigerant gradually changes from the liquid state to the gaseous state by absorbing heat from the medium to be cooled (heat source). The compressor is a mechanical device that sucks the gaseous refrigerant coming from the evaporator at low temperature and pressure, compresses it to a higher level of temperature and pressure and then delivers it to the condenser. The condenser is a heat exchanger that supplies the latent heat contained in the refrigerant in the gaseous state issuing from the compressor by liquefying it. The expansion valve reduces the temperature and the pressure of the refrigerant coming from the condenser before it is injected into the evaporator.

A plate heat exchanger (HX) is positioned between the air conditioner and the unit MD to recover the quantity of heat contained in the brine by preheating the feed solution and slow the progression of the feed temperature in the tank. A pump drives successively the feed solution in the cold channel of the MD unit, in the condenser of the air conditioning to heat the feed solution, then in the hot channel of the MD unit where the flux is divided between the permeate flux and the brine flux, which is slightly more concentrated in salt. The brine flows finally back to the feed tank. Pre-treatment and post-treatment are not dealt with in this study. The system is operated with mixed solutions of pure water and salts.

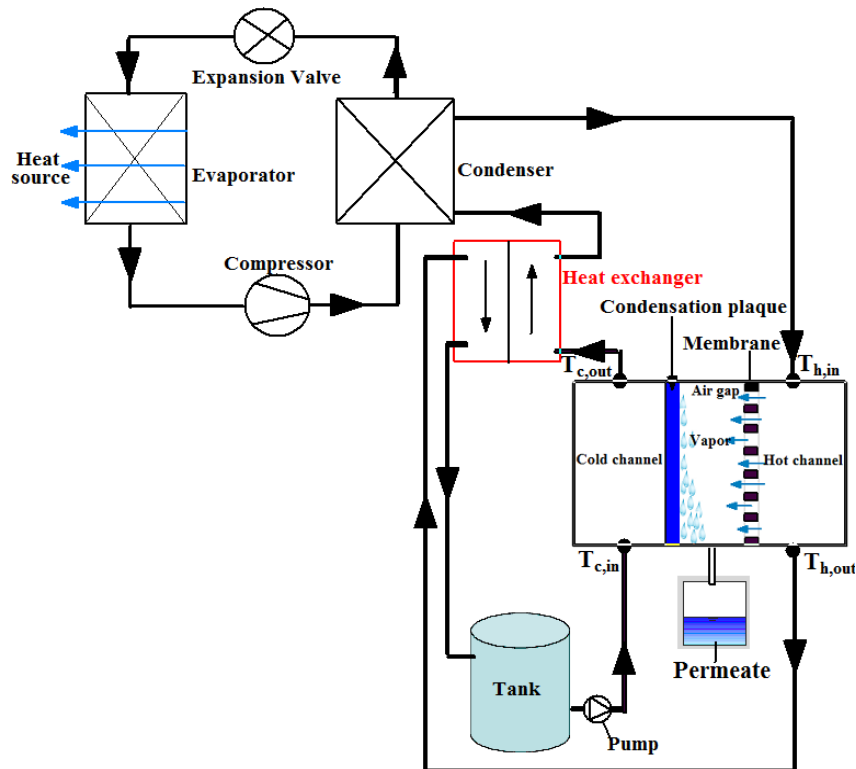


Figure 2: Scheme of the air conditioner coupled to the AGMD unit with heat exchanger (Scenario 2)

Two following scenarios are studied with this coupled system.

- In Scenario 1, the system is connected to a network of seawater instead of the water tank of Figure 2. The brine is directly discharged into the sea (open loop continuous operation). The recovery heat exchanger is used to preheat the feed seawater with the heat left in the brine. This scenario can be applied to hotels or office buildings installed close to the sea using refrigeration or air conditioning. The inlet temperature of the cold channel ($T_{c,in}$) is considered constant for a given test.

- Scenario 2 corresponds to the configuration shown in Figure 2 (batch mode). It is a system with a closed loop function that can be used in rural areas. The tank is assumed to be filled up regularly with a new amount of sea water or brackish water. An initial tank volume of 100 L was assumed acceptable regarding a daily filling up. A dynamic model is useful for evaluating the performance of the system because the salt concentration, the temperature and the mass of the reservoir evolve over time. A coefficient equal to 0.2 kW.K⁻¹ is applied to take into account the heat loss of the tank volume towards the environment because it continuously recovers the hotter brine.

3. Numerical modelling

3.1. Air conditioner model

The results of experimental tests on an air-to-water heat pump working with propane (R290) were used to validate the numerical models of the components [13]. The compressor power and the coefficient of performance (COP) are predicted within 5% of error. The coupled system is sized with a small air conditioner with nominal heating and cooling capacities of 2.5 kW and 2 kW respectively for T_{cd} = 40 °C and T_{ev} = 0 °C. The expansion valve is simply modelled by the conservation of the enthalpy through the expansion process. The models of compressor and heat exchangers are presented hereafter.

3.1.1. Compressor model

The compressor model is built using data tables provided by the manufacturer reporting the COP, the cooling capacity and the electric power consumption as a function of evaporating and condensing pressures. Equation 1 determines the refrigerant flow rate from the fluid density, volumetric efficiency and swept volume. Equation 2 is used to calculate the electrical power absorbed by the ideal mechanical power according to isentropic compression and the isentropic efficiency of the compressor.

$$\dot{W}_{is} = \rho \cdot \eta_{vol} \cdot \dot{V}_{swept} \cdot \Delta h_{comp} \quad (1)$$

$$\dot{W}_{comp} = \frac{\dot{W}_{is}}{\eta_{is}} \quad (2)$$

The volumetric and isentropic efficiency are given by equations 3 and 4 as a function of the compression ratio σ (ratio of high pressure over low pressure), evaporation and condensation temperatures and the polytropic coefficient γ .

$$\eta_{is} = -0,001\sigma^3 + 0,026\sigma^2 - 0,25\sigma - 0,014T_{ev} + 0,0108T_{cd} + 0,7512 \quad (3)$$

$$\eta_{vol} = -0,1290\sigma^\gamma + 0,1257\sigma + 0,9010 \quad (4)$$

3.1.2. Heat exchangers model

The heat exchanger models use the logarithmic average of the temperature difference method (DTLM). The heat exchanged can be calculated using equations 5 to 7. In the case of the external air evaporator, a correction factor F is taken into account due to cross-flow fluids. The resolution of the system of equations 5 to 7 makes it possible to calculate the refrigerant operating pressures as well as the outlet temperatures. The global heat exchange coefficients (U values for the evaporator and the condenser) were calculated using correlations on the convective heat exchange of the fluids as a function of their temperatures [14-15].

$$\dot{Q} = U \cdot S \cdot DTLM \quad (5)$$

$$\dot{Q} = \dot{m}_{so} \cdot C_{p_{so}} \cdot \Delta T_{so} \quad (6)$$

$$\dot{Q} = \dot{m}_r \cdot \Delta h_r \quad (7)$$

3.2. AGMD unit

In the AGMD configuration, the air gap is delimited by a microporous membrane and a condensation plate. A spacer is placed in the air gap to maintain the membrane at a constant distance of the condensation plate. Its thickness defines the permeate channel. Within the AGMD module, two phenomena occur simultaneously: heat and mass transfers. For modelling, it is possible to divide into four zones (Figure 3). The phenomenon was modelled using EES software. The 1D model was built using heat and mass transfer equations and literature correlations.

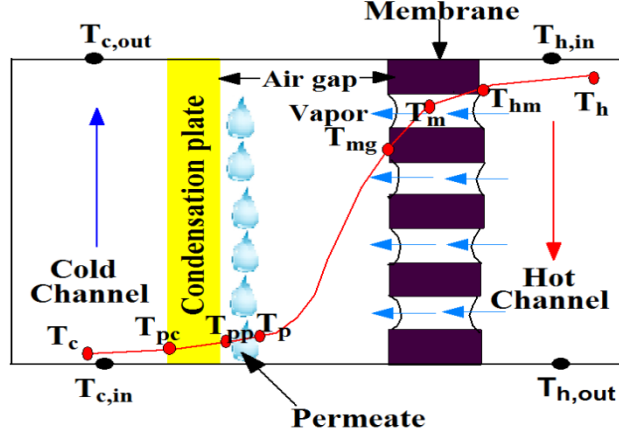


Figure 3: Mechanisms of heat and mass transfers in the AGMD unit

3.2.1. Heat transfer

Heat transfer by convection and conduction are the two modes of heat transfer generally dominating within an AGMD module. Heat transfer by radiation is most often neglected. Heat transfers takes place in the hot channel (i.e. between the hot feed solution and the surface of the membrane), inside the pores of the membrane, in the air gap, on the surface of the cold plate, in the cold channel and between the cold liquid and the surface of the cold plate. Energy conservation is applied in the unit (Equation 8). The amount of energy lost in the permeate flux and the heat losses through the plastic of the outside walls of the AGMD unit towards the surroundings are neglected.

$$\varphi_h = \varphi_m = \varphi_{ag} = \varphi_p = \varphi_c \quad (8)$$

The heat flux in the hot channel is a function of the convective exchange coefficient hc_h and of the temperature gradient between the temperature of the hot solution T_h and the temperature of the hot solution interface with the membrane T_{hm} (Equation 9). The temperature of the hot feed solution is calculated using the relation 10. Where $T_{h,in}$ and $T_{h,out}$ are input and output temperatures of the feed solution in the hot channel.

$$\varphi_h = hc_h (T_h - T_{hm}) \quad (9)$$

$$T_h = \frac{(T_{h,in} + T_{h,out})}{2} \quad (10)$$

The heat flux from the surface of the membrane to the condensate consists of a convective term and a diffusive term. It is governed by Equation 11, where R_{mT} is the thermal resistance of the membrane, T_{mg} is the temperature at the interface of membrane and air gap, J_v is the vapour flux passing through the membrane and Δh_v is the enthalpy of the vapour. The thermal resistance R_{mT} depends on the resistance of the membrane material R_m (equation 13) and the thermal resistance of the vapour in the pores R_v (equation 12). The resistance of the membrane can be calculated from the thermal conductivities of the material of the membrane k_m and air trapped inside the membrane pores k_a using equation 6 where δ_m and ε are the thickness and porosity of the membrane, respectively. The resistance of the vapour in the pores is calculated by Equation 14.

$$\varphi_m = \frac{1}{R_{mT}} (T_{hm} - T_{mg}) + J_v \Delta h_{ev} \quad (11)$$

$$R_{mT} = \frac{R_m R_v}{R_m + R_v} \quad (12)$$

$$R_m = \frac{\delta_m}{\varepsilon \cdot k_a + (1 - \varepsilon) \cdot k_m} \quad (13)$$

$$R_v = \frac{1}{J_v \cdot C p_v} \quad (14)$$

The heat flux through the air gap is assumed solely convective and carried by the water vapour and is calculated using equation 15 where R_{ag} and T_p are the thermal resistance of the air gap and temperature of permeate, respectively. The thermal resistance of the air gap can be calculated through equation 16. δ_{ag} , δ_p and δ_s are the air gap, permeate and spacer thicknesses, respectively. k_s is the conductivity of the spacer, V_{vs} is the void volume of the spacer and V_s is the total volume of the spacer. The permeate thickness is determined by equation 17, where ρ_w , ρ_v and μ_v are liquid water and vapour densities and vapour viscosity, respectively, and g is the acceleration of gravity.

$$\varphi_{ag} = \frac{1}{R_{ag}} (T_{mg} - T_p) \quad (15)$$

$$\frac{1}{R_{ag}} = \frac{1}{R_v} + \frac{(\delta_{ag} - \delta_p)}{k_a} + \frac{\delta_s}{(1 - V_{vs}/V_s) k_s} \quad (16)$$

$$\delta_p = \left[\frac{3 \mu_v \int_0^x J_v(x) dx}{g \rho_w (\rho_w - \rho_v)} \right]^{1/3} \quad (17)$$

The heat flux from the interface of the condensation surface to the interface between the cooling solution and the metal plate can be translated by equation 18 where k_p and δ_p are the thermal conductivity of the plate, the plate thickness and T_{pc} is the temperature at the interface of the cold solution and the plate.

$$\varphi_p = \frac{k_p}{\delta_p} (T_{pc} - T_p) + J_v \cdot \Delta h_{cd} \quad (18)$$

The heat flux in the boundary layer of the cold channel can be expressed by equation 19, where h_c and T_c are the heat transfer coefficient and the temperature of the cold solution in the cold channel. The mean temperature of the cold solution is calculated using equation 20.

$$\varphi_c = h c_c (T_p - T_c) \quad (19)$$

$$T_c = \frac{(T_{c,in} + T_{c,out})}{2} \quad (20)$$

The convective heat transfer coefficients $h c_h$ and $h c_c$ can be calculated by equation 21 where dh is the hydraulic diameter, k is the thermal conductivity and Nu is the Nusselt number and can be determined by the correlations of Table 2 depending on the Reynolds number.

$$h c = \frac{Nu k}{dh} \quad (21)$$

Table 2: Convective heat transfer coefficients used in the MD unit

Author	Correlation	Validity domain
Pangarkar [16]	$Nu = 0.023 Re^{0.8} Pr^{1/3} \left(\frac{\mu}{\mu_w} \right)^{0.14}$	$2500 < Re < 1.25 \cdot 10^5$
Aryapratama [17]	$Nu = 3.36 + \frac{0.036 Re Pr (dh/L)}{1 + 0.0011 (Re Pr/L)^{0.8}}$	$Re > 2100$
Khayet [18]	$Nu = 0.116 (Re^{1/3} - 125) Pr^{1/3} [1 + (dh/L)^{2/3}]$	Transitional regime
Phattaranawik [19]	$Nu = 0.664 Re^{0.5} Pr^{0.33} (dh/L)^{0.5}$	
Essalhi [20]	$Nu = 1.86 (Re Pr dh/L)^{1/3}$	Laminar flow regime

3.2.2. Mass transfer

Mass transfer through the membrane depends on the vapour pressure difference between the two sides of the membrane. The relationship between the mass transfer, the vapour pressure difference and the effect of salt concentration in the solution is given by equation 22, where P_{hm} and P_p are the vapour pressures at the surface of the membrane in the boundary layer of the hot channel and in the air gap near the surface of the cold plate, respectively. α is the activity coefficient and β is the water fraction of the solution. Pressures P_{hm} and P_p can be evaluated using the Antoine equation (equation 23). The activity coefficient α of an aqueous solution can be calculated by equation 24. The permeability of the membrane or the mass transfer coefficient B_w of equation 22 is given in equation 25. M_w , R^* , T_m and P are the molecular weight of water, the gas constant, the absolute temperature of the membrane and the total pressure inside the pores, respectively. D_{va} is the thermal diffusivity of water vapour in the air gap and τ is the tortuosity of the membrane and can be calculated by equation 26. The product PD_{va} can finally be calculated by equation 27.

$$J_w = B_w(\alpha \beta P_{hm} - P_p) \quad (22)$$

$$P = \exp\left(23,1964 - \frac{3816,44}{T - 46,13}\right) \quad (23)$$

$$\alpha = 1 - 0,5 X_{NaCl} - 10 X_{NaCl}^2 \quad (24)$$

$$B_w = \frac{\varepsilon M_w P D_{va}}{R^* T_m (\delta_m \tau + \delta_{ag}) |P_a|_{ln,a}} \quad (25)$$

$$\tau = \frac{2 - \varepsilon}{\varepsilon} \quad (26)$$

$$PD_{va} = 1,895 \times 10^{-5} T_m^{2,027} \quad (27)$$

The mass balance of the AGMD module is given by equation 28, where $\dot{m}_{sw,in}$, $\dot{m}_{sw,out}$ and \dot{m}_p are the mass flow rate, feed solution inlet, feed solution out and permeate, respectively.

$$\dot{m}_{sw,in} = \dot{m}_{sw,out} + \dot{m}_p \quad (28)$$

3.2.3. Dynamic behaviour

In Scenario 2 (see section 2), the mechanisms of heat and mass transfers strongly depend on the initial mass and the initial temperature of the water tank. The evolution of these quantities is a function of time for the system studied. The mass of the tank is calculated as following:

$$m_{tank} = m_{i,tank} - \int_0^t \dot{m}_p dt \quad (29)$$

The heat transfer in the balance tank containing the feed is estimated by equation 30. The UA_{tank} value is the product of a heat exchange coefficient and a surface area evaluating the heat losses of the tank.

$$Cp_{tank} \Delta T \frac{dm_{tank}}{dt} = - \dot{m}_{f,in} Cp_{f,in} T_{f,in} + \dot{m}_{f,out} Cp_{f,out} T_{f,out} - UA_{tank} (T_{tank} - T_{amb}) \quad (30)$$

The evolution of the tank temperature can be calculated by equation 31. $T_{i,tank}$ corresponds to the initial temperature of the feed solution in the tank.

$$T_{tank} = T_{i,tank} + \int_0^t \frac{\Delta T}{\delta t} dt \quad (31)$$

The water salinity in the tank also varies with time. During the operation, distilled water is produced. This amount of water does not reintegrate the water tank while the amount of salts stays constant because on the contrary, the brine flows back to the tank. Equation 32 calculates the evolution of the salinity with time.

$$S = \frac{m_{sw}}{m_{tank}} \quad (32)$$

3.3. System performance assessment

3.3.1. Cooling device

In these studies, the compressor consumption and the coefficient of performance (COP) are evaluated. We define the COP as the ratio of the cooling capacity to the electric power absorbed by the compressor (equation 33).

$$COP = \frac{\Phi_{ev}}{\dot{W}_{elec}} \quad (33)$$

3.3.2. Desalination unit

For desalination units, the performance is evaluated by the amount of energy consumed with respect to the amount of freshwater produced. The GOR (Gained Output Ratio) corresponds to the ratio of the amount of energy necessary to vaporize the permeate flux divided by the heat consumption GOR is used to measure the energy consumption of the process and it can be described by [21] (equation 34).

$$GOR = \frac{\dot{m}_p \Delta h_v}{\dot{m}_{sw,in} c_{p,sw,in} (T_{h,in} - T_{h,out})} \quad (34)$$

3.3.3. Exergy analysis

An exergy analysis is performed to convert the energy amounts from different forms (thermal, electric, chemical) and to calculate an exergy efficiency [22]. The exergy rate available in a water flux comprises thermal and chemical (e^{ch}) terms and is evaluated by equation 35. This equation can be used to determine the exergy rate of the brine $\dot{E}x_{sw,out}$. The exergy rate of a thermal flux $\dot{E}x_{th}$, such as the cooling energy, is calculated using equation 36. The reference state is defined by mean ambient conditions ($T_0 = 20$ °C and $P_0 = 1$ bar). The exergy efficiency of the system is given by equations 37 and 38. The economical exergy efficiency takes into account the useful production and the charged inputs to the system. The process exergy efficiency regards all inputs and outputs with the idea that every stream has a potential value.

$$\dot{E}x_w = \dot{m} \left[(h - h_0) - T_0 (s - s_0) + e^{ch} \right] \quad (35)$$

$$\dot{E}x_{th} = \Phi_{ev} \left| 1 - \frac{T_0}{\bar{T}} \right| \quad (36)$$

$$\eta_{ex,eco} = \frac{\dot{E}x_{th} + \dot{E}x_{w,out}}{\dot{E}x_{elec} + \dot{E}x_{pump}} \quad (37)$$

$$\eta_{ex,pro} = \frac{\dot{E}x_{th} + \dot{E}x_{w,out} + \dot{E}x_{sw,out}}{\dot{E}x_{elec} + \dot{E}x_{pump} + \dot{E}x_{sw,in}} \quad (38)$$

4. Results and discussion

4.1. Experimental results

The experimental tests were carried out on an AGMD pilot plant (Xzero AB, Sweden) (Figure 4). The pilot plant is equipped with a 25-litre feed tank and a PTFE membrane (Gore, USA) with the same characteristics as reported in Table 3 and with a surface area of 0.195 m². Several parameters were studied, such as hot feed temperature, feed and coolant flow rates and air gap thickness with a model solution at 35 g/l NaCl. The feed temperature varies from 25 to 65 °C. The range of feed flow rate and coolant flow rate is from 2 to 5 l/min. The air gap thickness is 1.04 mm. The mean temperature of the cold fluid is the one of the chilled water network of the building, at 16 °C for all tests. The permeate is sampled every 20 minutes and then weighed with a precision scales. The permeate conductivity κ_p is measured with a conductivity meter in order to calculate the salt rejection using equation 39.

$$salt\ rejection = \frac{\kappa_{sw,in} - \kappa_p}{\kappa_{sw,in}} \quad (39)$$

Table 3: Membrane characteristics (according to supplier)

Property	Value
Thickness (mm)	0.28
Pore size (μm)	0.2
Porosity ε (%)	80
Tortuosity τ (-)	1.5

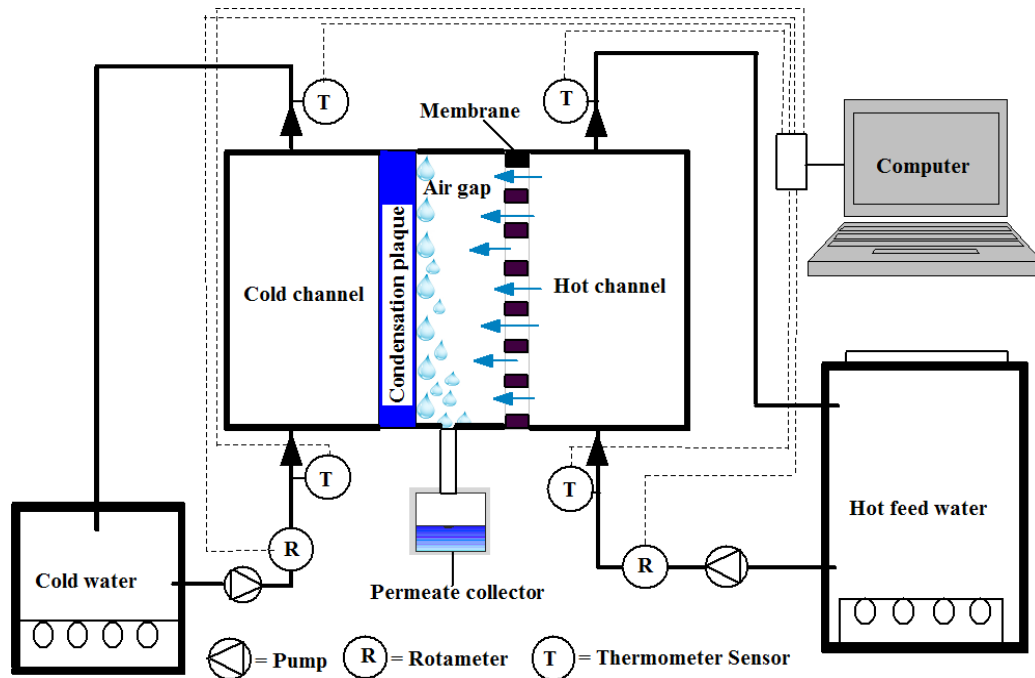


Figure 4: Scheme of the AGMD pilot plant

4.1.1. Long term performance

A test of a total operating time of about 30 hours was performed during four consecutive days with real seawater sampled in St Malo, France. For this long-term test, the same quantity of seawater as the produced permeate mass is added to the initial seawater in the tank every 20 minutes. This method concentrates the hot feed solution. Figure 5 shows the evolution of the electrical conductivity in the reservoir containing the feed solution.

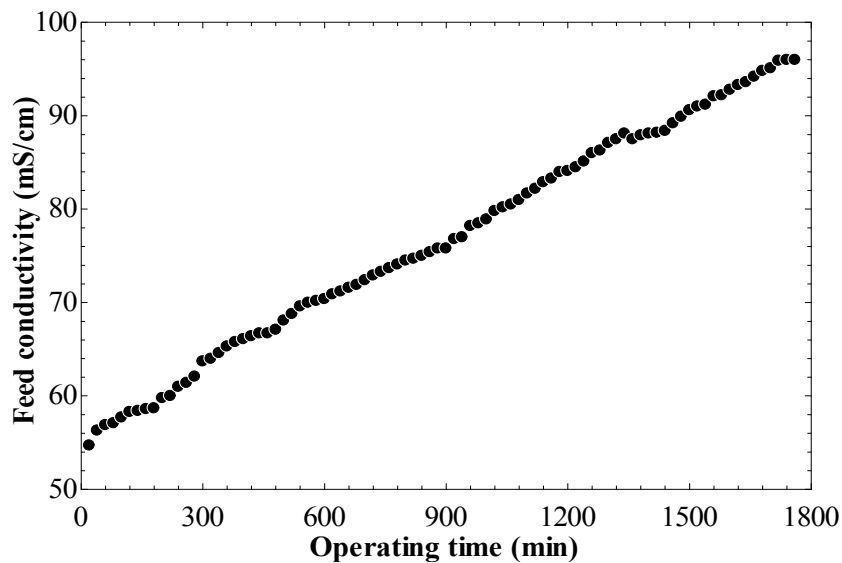


Figure 5: Evolution of the conductivity of the feed solution in the tank

During these tests, the temperature of the hot feed is maintained at 45 °C, 5 and 2 l/min are the hot and cold flow rates, respectively. Under these conditions, the long-term operation appears relatively stable. The permeate flux decreases from 2.56 to 2.17 kg/m²h (i.e. a decrease of 15.6 %) with a salt rejection over 99.99 % (Figure 6). The distillate produced by the MD decreases with increasing salt content. Despite the increase in electrical conductivity, the salt rejection rate remains quasi-stable. Lower values (but > 99.96%) of salt rejection appear for the first sample each day. These long-term tests provide essential results on the fact that the membrane operates correctly and that the process can be run in a batch mode. Therefore, Scenario 2 seems a credible solution for unconnected areas.

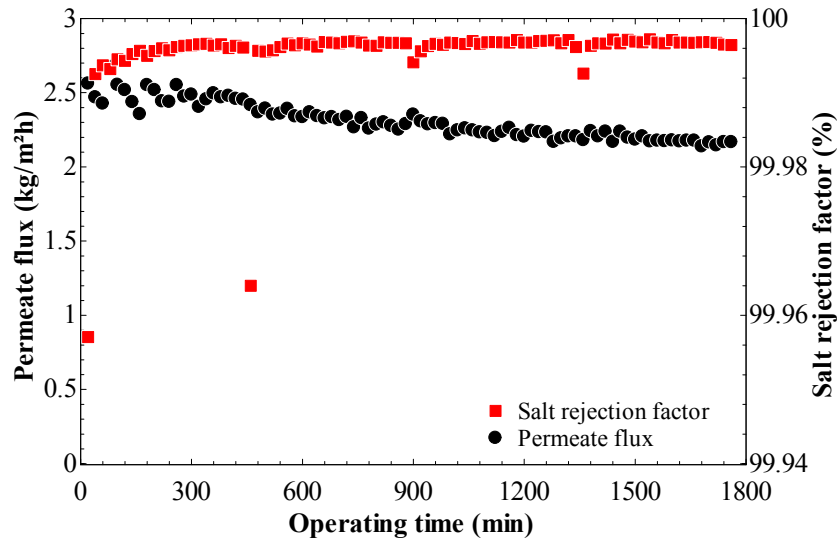


Figure 6: Evolution of the permeate flux and the salt rejection

4.1.2. Validation of the AGMD theoretical model

Figure 7 shows the comparison of the experimental and theoretical data of the permeate flux. These curves are obtained with an air gap of 1.04 mm and flow rates of hot and cold fluids of 2 l/min and 5 l/min. These flow rate values are the lowest and the highest that can be obtained with the control capacities of the pilot. During the validation, the hot feed temperatures are varied from 25 to 65 °C. The maximum error between experimental and theoretical values is $\pm 6\%$. This model can thus be implemented for simulation of the coupled system.

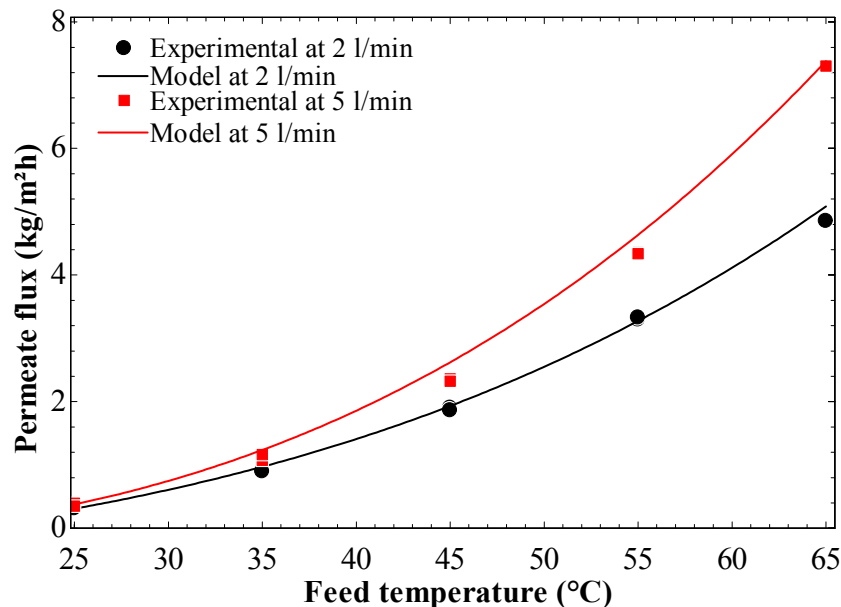


Figure 7: Comparison of permeate fluxes between theoretical model prediction and experimental results for the AGMD pilot plant

4.2. Simulation results with the coupled system

The results of the coupled system are calculated with a membrane area of 1 m². The properties of the membrane remain the same as in Table 3.

4.2.1. Effect of the heat source temperature at the evaporator of the cooling device

The effect of the heat source temperature of the cooling device is evaluated using Scenario 1. The heat source varies from -10 °C to 25 °C, with an air gap thickness of 1.04 mm an flow rate of 2 l/min and different initial tank feed temperatures. Figure 8 shows the permeate flux as a function of the temperature of the heat source and the initial feed temperature of the tank. The permeate flux is very sensitive to the variation of the heat source temperature. It is observed that the permeate flux increases as the heat source temperature increases. If the ambient air temperature increases, the refrigerant evaporates at a higher temperature, this will allow the compressor to draw in the refrigerant without consuming a too high amount of electrical energy. When the temperature of the heat source decreases, the COP, the cooling and heating capacities decrease because the compressor consumes more of its energy to build up pressure than to send refrigerant flow rate. The MD unit receives colder seawater in the hot channel and the temperature and vapour gradient is lower. Therefore, the permeate flux decreases with the lower cooling capacity when considering the same refrigerating machine. This result shows that air conditioning is more suitable than domestic cooling and refrigeration for a large permeate flux production. In the following simulations, the air inlet temperature will be fixed at 25 °C (i.e. in the case of an air conditioner).

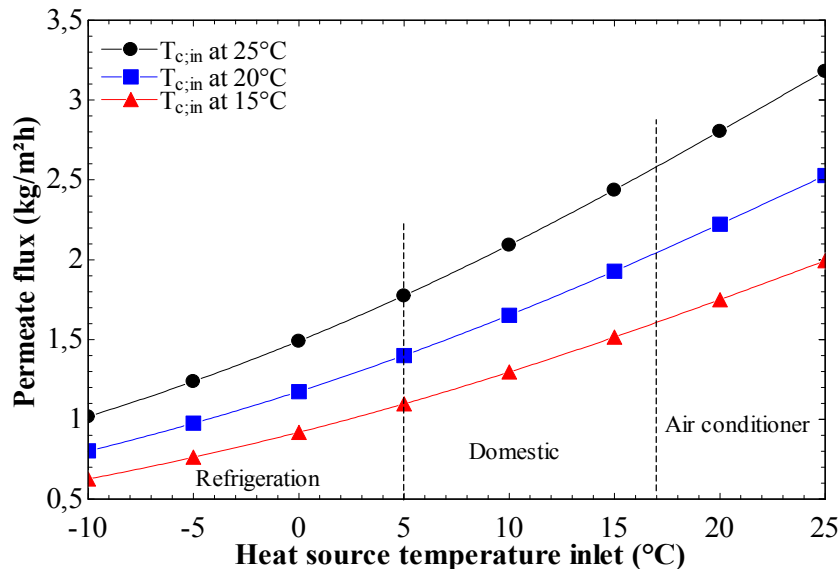


Figure 8: Simulated effect of air temperature of the refrigerating device on the permeate flux

4.2.2. Effect of the flow rate and the feed inlet temperature

Figure 9 shows the effect of the seawater inlet temperature on the outlet temperature of the condenser of the cooling device and the permeate flux at a flow rate of 2 and 5 l/min. Different sea water temperatures (15 to 30 °C) were used to observe the behaviour of the coupled system studied. Figure 9a shows that the feed inlet temperature increases the inlet temperature in the hot channel. The condenser outlet temperatures are higher for the lower feed flow rate. This is due to the fact that the residence time of the feed solution is longer when the flow rate is lower. This results in an increase of the permeate flux (Figure 9b). The increase of the permeate flux is exponential with respect to the feed inlet temperature in the hot channel. This result can be seen in Figure 7 in the experimental validation work of the numerical model of the AGMD. Furthermore, the permeate flux is sensitive to the variation of the initial inlet temperature of the cold channel. The driving force behind the mass transfer in the AGMD process increases when the outlet temperature of the condenser (or feed inlet temperature in the hot channel) increases, which leads to an increase of the transmembrane vapour pressure gradient in accordance with the Antoine equation (equation 23). When the inlet temperature of the cold channel increases from 15 to 30 °C, the permeate flux is almost twice for a flow rate of 2 l/min. For a decrease of the flow rate of 5 to 2 l/min, there is an increase of 70.9 % with an inlet temperature of the cold channel of 30 °C.

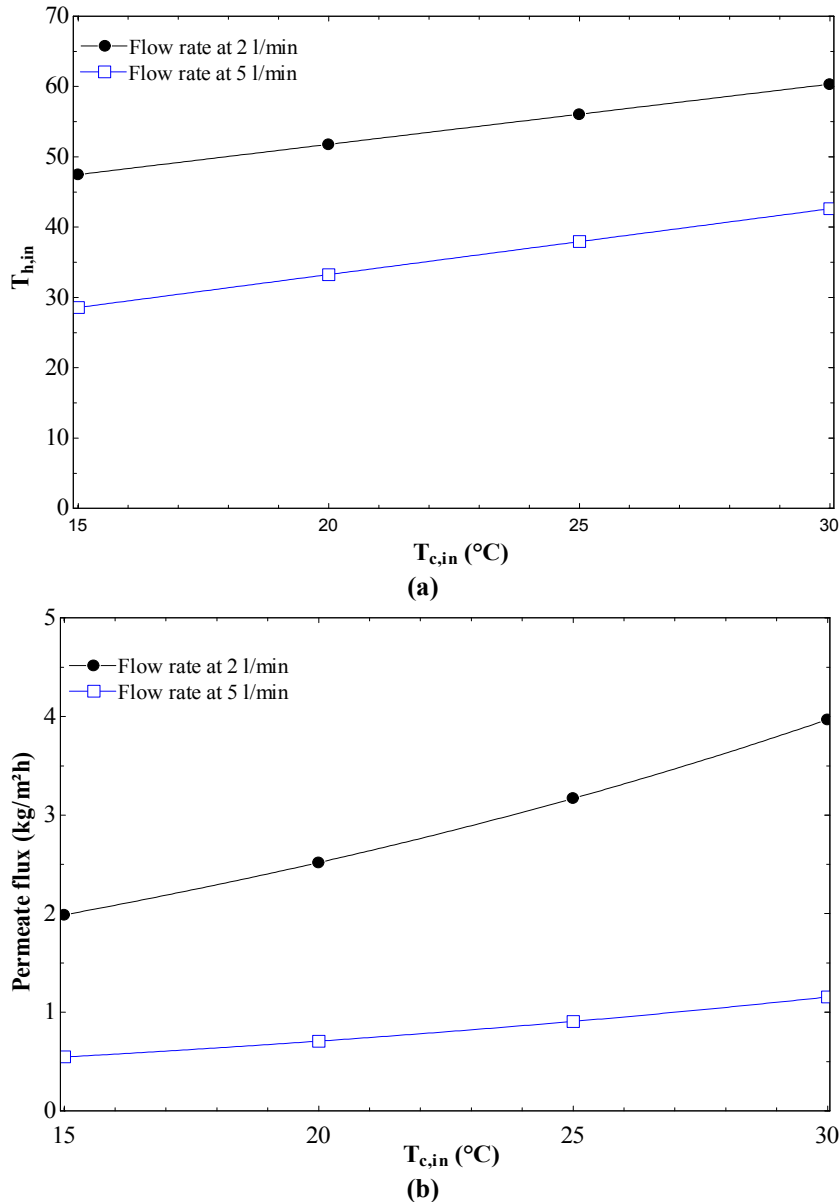


Figure 9: Simulated effect of feed temperature inlet cold channel and flowrate on (a): Feed temperature inlet in the hot channel and (b): Permeate flux (Scenario 1)

In Scenario 2, a tank capacity of 100 L is chosen to expect to desalinate a substantial part of the water consumption of one person per day. The initial salinity of the feed water in the tank is 35 g/kg, corresponding to the average salinity of Atlantic Ocean, with an initial temperature of 15 °C. In this simulation condition, the evolution of the inlet temperature of the hot channel and that of the tank are shown in Figure 10 for a duration of 420 minutes of continuous operation. This duration corresponds to 7 hours, which is a reasonable operating time per day for an air conditioning unit. It is observed that the temperature of the tank is not very sensitive to the variation of the flow rate. Nevertheless, a high flow rate increases this temperature. It is also visible in Fig 10 that a lower flow rate produces a higher feed inlet temperature at the hot channel for the same reason mentioned in Scenario 1 (Figure 9a). As the temperature of the water tank increases with time, it also raises the condenser outlet feed temperature. After 120 minutes of operation, the temperatures stabilize because the heat gained by the brine return is balanced by the heat losses of the tank towards the environment. Figure 11 illustrates the production of permeate flux and the effect of salt concentration. It is evident that the salt concentration increases more rapidly with a low flow rate (Figure 11) because the latter produces more demineralized water. This increase in salt concentration decreases the permeate flux compared to Figure 7 because the surface area of the membrane used and the $T_{h,in}$ are lower with the experimental test. The freshwater masses produced after 420 minutes of operation with 2 and 5 l/min are 33.9 and 21.0 kg respectively. In comparison, Scenario 1, run in a continuous mode, is not influenced by salinity variation. However, the feed water temperature is limited to the sea temperature. The higher permeate

flux, being constant over time, enables to produce, in 420 minutes, only 27.9 and 8.0 kg with 2 and 5 l/min respectively. These values are obtained with a feed water temperature of 30 °C, which is lower than in Scenario 2.

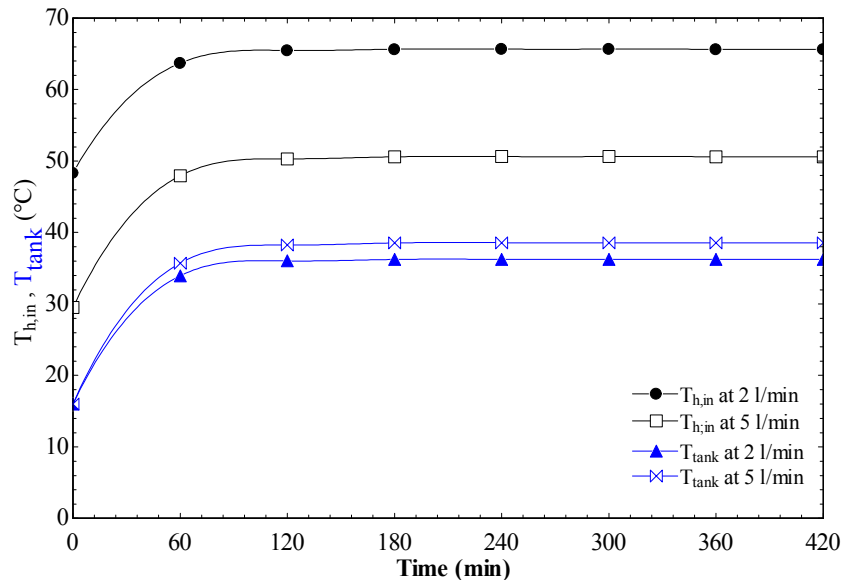


Figure 10 Simulated effect of flow rates on tank and hot feed inlet temperatures (Scenario 2)

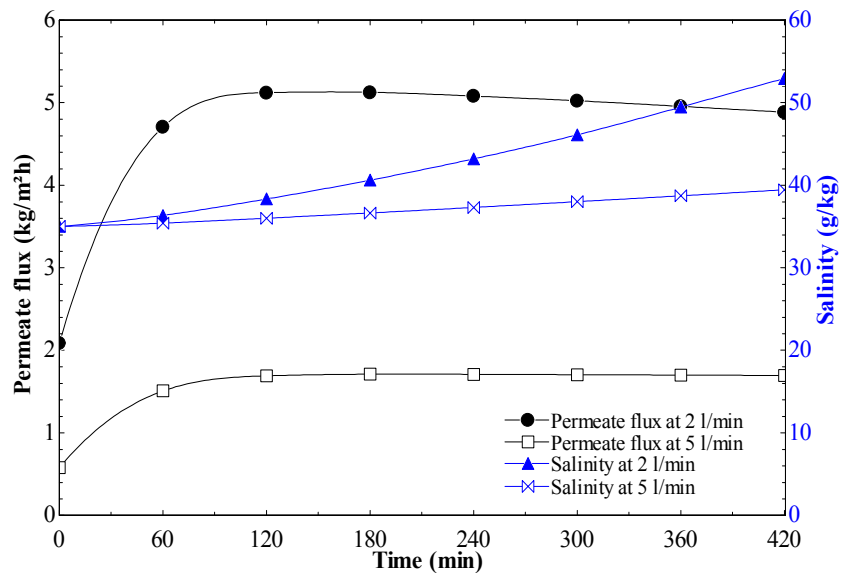


Figure 11: Simulated effect of flow rates on permeate flux and water tank salinity (Scenario 2)

4.2.3. Performance of the system

The COP, the GOR and the exergy efficiency are used to evaluate the performance of this system. The COP characterizes the performance of the air conditioner and the GOR, that of the MD. The COP of the air conditioner decreases considerably with the flow rate (Figures 12 and 13). For Scenario 1, an increase of the temperature of the seawater feed in the cold channel of the MD unit also reduces the COP as shown in Figure 12. In Scenario 2, the inlet temperature of the cold channel corresponds to the change in the temperature of the tank over time. As the temperature of the water tank stabilizes in 120 minutes of operation (Figure 10), this behaviour is constant with the COP (Figure 13). A decrease of the COP may penalize the functioning of the heat pump by increasing the power consumption of the compressor for the same cooling duty.

The GOR is also present in figures 12 and 13 respectively for Scenario 1 and Scenario 2. The GOR increases with the increase of $T_{c,in}$ or T_{tank} and $T_{h,in}$. When the temperature inlet of the cold channel increases, this results in a small decrease of the temperature difference, which means that it requires less heat to reach the required

temperature. This secondary effect is added to the significant increase of the permeate flux to generate an improvement of GOR. The maximal value of the GOR is of 7.4 at 2 l/min and $T_{c,in} = 30\text{ }^{\circ}\text{C}$ for Scenario 1. In Scenario 2, the GOR reaches 9.8 with a flow rate of 2 l/min for an operating time of 120 min. After this time, the higher salinity shown in Figure 11 slightly reduces the permeate flux and the GOR.

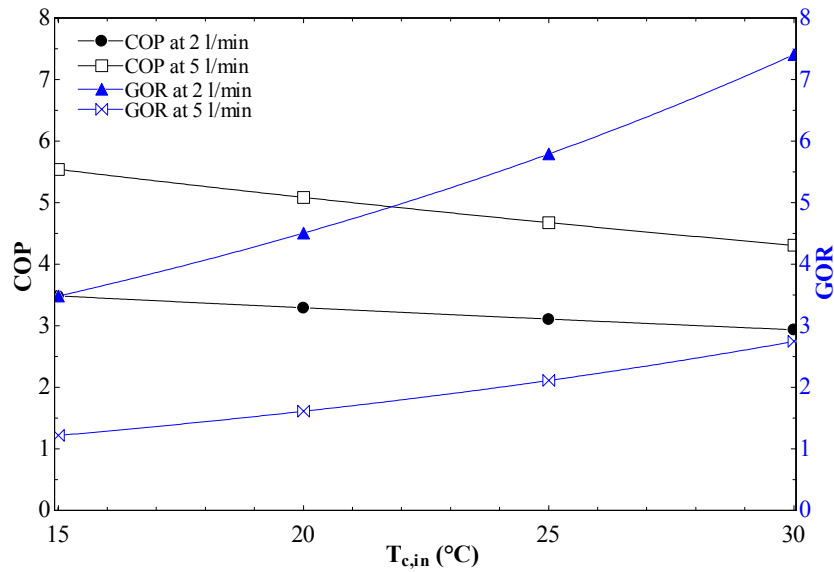


Figure 12: Simulated effect of feed temperature inlet cold channel and flow rate on COP and GOR (Scenario 1)

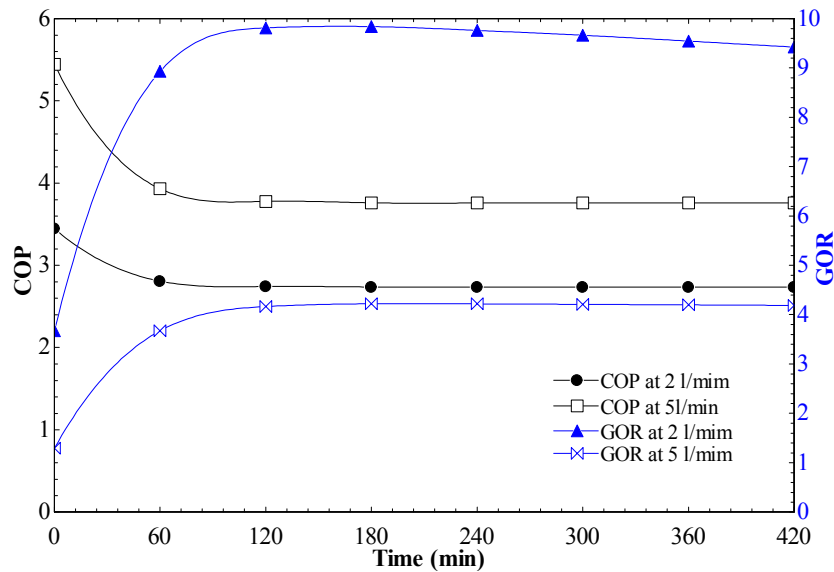


Figure 13: Simulated effect of flow rates on COP and GOR (Scenario 2)

An exergy analysis was performed to evaluate the irreversibility of the system using the second law of thermodynamics. Exergy corresponds to the amount of equivalent mechanical work available of other forms of energy. Electric energy is considered as pure exergy. Table 4 shows the detailed results of exergy rates and economical and process exergy efficiencies for Scenario 1 and Scenario 2. The exergy rate of the pump is considered constant and equal to 50 W for Scenario 1 and 5 W for Scenario 2. Scenario 1 supposes to pump the seawater from the sea. Therefore, the pipe length and the pressure drops require a more powerful pump. In both scenarios, the process exergy efficiency including exergy amounts from feed seawater and brine increases progressively as $T_{c,in}$ (in Scenario 1) or T_{tank} (in Scenario 2) increases. However, the higher exergy efficiencies on an economical viewpoint are found for the higher flow rate and the lower temperatures in both scenarios. This result is mainly explained by the fact that the electric power consumed by the compressor is lower.

Table 4: Exergy analysis of individual components

Scenario	Flow rate [l/min]	T _{c,in} , T _{tank} [°C]	Ex _{elec} [kW]	Ex _{th} [kW]	Ex _{sw,out} [kW]	Ex _{w,out} [kW]	Ex _{sw,in} [kW]	η _{ex,eco} [%]	η _{ex,pro} [%]
1	2	15	0.797	0.248	0.008	0.034	0.006	30.0	33.7
		20	0.822	0.244	0.000	0.063	0.006	28.7	35.9
		25	0.847	0.238	0.004	0.099	0.025	29.3	40.2
		30	0.871	0.232	0.020	0.142	0.052	30.8	45.3
	5	15	0.596	0.251	0.019	0.006	0.003	39.3	39.0
		20	0.632	0.255	0.000	0.038	0.001	37.4	43.0
		25	0.668	0.256	0.011	0.095	0.006	36.5	49.0
		30	0.704	0.256	0.052	0.176	0.013	35.8	55.3
2	2	15.0	0.797	0.248	0.008	0.034	0.006	31.7	35.6
		33.8	0.889	0.227	0.040	0.180	0.081	34.4	52.1
		36.0	0.899	0.223	0.054	0.203	0.100	35.8	54.9
		36.2	0.900	0.223	0.067	0.219	0.097	35.3	55.4
	5	15.0	0.596	0.251	0.019	0.006	0.003	42.2	41.9
		35.6	0.743	0.254	0.129	0.293	0.026	37.5	65.5
		38.2	0.761	0.253	0.177	0.359	0.035	37.5	68.4
		38.6	0.764	0.253	0.185	0.369	0.035	37.4	68.8

5. Conclusion

A model of air conditioner operating with propane (R290) is used in this work for a coupling with an AGMD unit. The model results were compared with experimental data from an AGMD pilot plant. The long-term experiments show a constant salt rejection rate over 99.99% that validates the quality of the membrane and the process.

The effects of various operating parameters such as feed water temperature and flow rate on the permeate flux were studied and presented in this study. The analysis showed that the temperature outlet of the feed water is high when the residence time of the water is long inside the heat exchanger (condenser). It leads to a higher permeate flux. However, low flow rates and high cold channel inlet temperatures reduce the COP of the air conditioner but conversely, they increase the GOR in the two scenarios studied. In Scenario 1, the exergy efficiency is better with a high flow rate and low cold channel inlet temperature. In Scenario 2, increasing the temperature of the water tank seems to reduce the exergy efficiency for a long period of operation of the air conditioner. One advantage of Scenario 1 is that the salt concentration is constant and does not influence the permeate flux. In Scenario 2, the permeate flux decreases over time by the salt concentration in the water tank. This Scenario 2 can be improved in the future by reducing as much as possible the temperature of the tank.

The set of results presented here is interesting as being a first assessment of design parameters for an MD unit system coupled to an air conditioner. It confirms that the two scenarios can be envisaged for either coastal buildings or remote areas.

Nomenclature

A: surface area [m²]
B_w: mass transfer coefficient [kg/m²·h·Pa]
C_p: thermal capacity [J/kg·K]
D_{va}: thermal diffusivity of water vapour in air [m²/s]
d_h: hydraulic diameter [m]
e: specific exergy [J/kg]
Eẋ: exergy rate [W]
h_c: convective heat transfer coefficient [W/m²·K]
h: specific enthalpy [J/kg]
HP: heat pump
J: flux [kg/m²·s]
k: thermal conductivity [W/m·K]
L: module length [m]
ṁ: mass flow rate [kg/s]
Nu: Nusselt number [-]
P: pressure [Pa]

Pr: Prandtl number [-]
 φ : thermal flux [W/m²]
 Φ : thermal capacity [W]
Re: Reynolds number [-]
R: thermal resistance [m²·K/W]
R*: Gas constant [J/K·mol]
R290: propane
s: specific entropy [J/kg·K]
S: salinity [g/kg]
T: temperature [°C]
t: time [s]
 \dot{V} : (swept) volume [m³/s]
U: heat transfer coefficient [W/m²·K]
 \dot{W} : power [W]
X: mole fraction [-]

Greek letters

α : activity coefficient [-]
 β : water fraction [-]
 δ : thickness [m]
 ε : porosity [-]
 η : efficiency [-]
 κ : electric conductivity [S/m]
 μ : dynamic viscosity [kg/m·s]
 ρ : density [kg/m³]
 σ : compression ratio [-]
 τ : tortuosity [-]

Subscripts

0: reference state
a: air
ag: air gap
c: cold
cd: condenser
ch: chemical
elec: electric
ev: evaporator
ex: exergy
f: feed
h: hot
hm: hot fluid - membrane interface
HX: exchanger heat
in: inlet
is: isentropic
m: membrane
ma: membrane - air gap interface
NaCl: sodium chloride
out: outlet
p: permeate
pc: cold fluid - plate interface
pp: temperature at permeate - plate interface
r: refrigerant
s: spacer
so: source
sw: seawater
th: thermal
v: vapour
vs: void in the spacer
w: water

Acknowledgements

The authors would like to acknowledge the financial supports of this project by Région Bretagne and Fondation de la Banque Populaire de l'Ouest.

References

- [1] Website of the French refrigeration association: www.aff.fr
- [2] HLPE, L'eau, enjeu pour la sécurité alimentaire mondiale. Rapport du Groupe d'experts de haut niveau sur la sécurité alimentaire et la nutrition du Comité de la sécurité alimentaire mondiale, Rome 2015
- [3] P. Byrne, L. Fournaison, A. Delahaye, Y. Ait Oumeziane, L. Serres, P. Loulergue, A. Szymczyk, D. Mugnier, J.-L. Malaval, R. Bourdais, H. Gueguen, O. Sow, J. Orfi, T. Mare. A review on the coupling of cooling, desalination and solar photovoltaic systems. *Renewable and Sustainable Energy Reviews* 47 (2015) 703–717
- [4] P. Byrne, Y. Ait Oumeziane, L. Serres, J. Miriel, Numerical Study of a membrane distillation unit for desalination coupled to a heat pump, *Applied Mechanics and Materials* 819 (2016) 152-159
- [5] R. Gonzalez-Bravo, N. A. Elsayed, J. M. Ponce-Ortega, F. N. Apoles-Rivera, M. M. El-Halwagi, Optimal design of thermal membrane distillation systems with heat integration with process plants, *Applied Thermal Engineering* 75 (2015) 154 – 166
- [6] C. Charcosset, A review of membrane processes and renewable energies for desalination, *Desalination* 245 (2009) 214-231
- [7] E. Drioli, Y. Wu and V. Calabro, Membrane distillation in the treatment of aqueous solutions, *Journal of Membrane Science*, 33 (1987) 277-284
- [8] P. Wang, T.-S. Chung, Recent advances in membrane distillation processes: Membrane development, configuration design and application exploring, *Journal of Membrane Science* 474 (2015) 39 – 56
- [9] R. Tian, H. Gao, X.H. Yang, S.Y. Yan, S. Li. A new enhancement technique on air gap membrane distillation, *Desalination* 332 (2014) 52-59
- [10] E. K. Summers, V.J.H. Lienhard, Experimental study of thermal performance in air gap membrane distillation systems, including the direct solar heating of membranes, *Desalination* 330 (2013) 300-311.
- [11] M.A.E.-R. Abu-Zeid, Y. Zhang, H. Dong, L. Zhang, H.-L. Chen, L. Hou, A comprehensive review of vacuum membrane distillation technique, *Desalination* 356 (2015) 1–14
- [12] S. Klein, Engineering Equation Solver, Version 10.200-3D, ©1992-2017
- [13] R. Ghoubali, P. Byrne, F. Bazantay, Simulation study of heat pumps for simultaneous heating and cooling coupled to buildings. *Energy and Buildings* 72 (2014) 141–149
- [14] American Society of Heating, Refrigerating and Air Conditioning Engineers, ASHRAE Handbook, Fundamentals, SI Edition (1989)
- [15] J. Navarro-Esbri, F. Moles, B. Peris, A. Barragan-Cervera, M. Mendoza-Miranda, A. Mota-Babiloni, J.M. Belman, Shell-and-tube evaporator model performance with different two-phase flow heat transfer correlations. Experimental analysis using R134a and R1234yf, *Applied Thermal Engineering* 62 (2014) 80–89
- [16] B. L. Pangarkar, S. K. Deshmukh, Theoretical and experimental analysis of multi-effect air gap membrane distillation process (ME-AGMD), *Journal of Environmental Chemical Engineering* 3 (2015) 2127–2135.
- [17] R. Aryapratama, H. Koo, S. Jeong, S. Lee, Performance evaluation of hollow fiber air gap membrane distillation module with multiple cooling channels, *Desalination* 385 (2016) 58–68
- [18] M. Khayet, Membranes and theoretical modeling of membrane distillation: A review, *Advances in Colloid and Interface Science* 164 (2011) 56–88
- [19] J. Phattaranawik, R. Jiraratananon, A.G. Fane, C. Halim, Mass flux enhancement using spacer filled channels in direct contact membrane distillation, *Journal of Membrane Science* 187 (2001) 193–201
- [20] M. Essalhi, M. Khayet, Application of a porous composite hydrophobic/hydrophilic membrane in desalination by air gap and liquid gap membrane distillation: A comparative study, *Separation and Purification Technology* 133 (2014) 176–186
- [21] A. Khalifa, H. Ahmad, M. Antar, T. Laoui, M. Khayet, Experimental and theoretical investigations on water desalination using direct contact membrane distillation, *Desalination* 404 (2017) 22–34
- [22] F. Macedonio, E. Drioli, An exergetic analysis of a membrane desalination system, *Desalination* 261 (2010) 293–299